Gravity Wave and Tidal Structures between 60 and 140 km Inferred from Space Shuttle Reentry Data

DAVID C. FRITTS

Laboratory for Atmospheric and Space Physics and Electrical and Computer Engineering Department, University of Colorado, Boulder, Colorado

DING-YI WANG

Institute for Space and Terrestrial Sciences, North York, Ontario, Canada

ROBERT C. BLANCHARD

NASA Langley Research Center, Hampton, Virginia

(Manuscript received 20 December 1991, in final form 11 May 1992)

ABSTRACT

This study presents an analysis of density measurements made using high-resolution accelerometers aboard several space shuttles at altitudes from 60 to 140 km during reentry into the earth's atmosphere. The observed density fluctuations are interpreted in terms of gravity waves and tides and provide evidence of the importance of such motions well into the thermosphere. Height profiles of fractional density variance reveal that wave amplitudes increase at a rate consistent with observations at lower levels up to ~90 km. The rate of amplitude growth decreases at greater heights, however, and appears to cease above ~110 km. Wave amplitudes are nevertheless large at these heights and suggest that gravity waves may play an important role in forcing of the lower thermosphere.

1. Introduction

In a previous study, Fritts et al. (1989) used the density fluctuations measured with high-resolution accelerometers during several space shuttle reentries to examine the amplitudes and horizontal wavenumber spectra of the gravity wave field at altitudes of 60 to 90 km. The purpose of this paper is to extend that analysis to greater heights and use this unique dataset to assess the possible roles of such motions in the lower thermosphere.

The importance of gravity waves and tides in forcing the large-scale circulation and structure of the middle atmosphere is now well established. Gravity waves provide strong forcing of the local mean flow by virtue of their amplitude growth with height and their dissipation through instability and wave–wave and wave–mean flow interaction processes (Fritts 1984, 1989; Dunkerton 1989). These result in the divergence of the vertical flux of horizontal momentum and energy and their associated accelerations, induced mean motions, turbulent diffusion, and departures from radiative equilibrium conditions (Vincent and Reid 1983; Thrane et al. 1985; Fritts and Yuan 1989; Tsuda et al. 1990; Garcia 1989; McIntyre 1989; Rüster and Reid 1990; Wang and Fritts 1990; Blix et al. 1990). Tidal motions likewise achieve large amplitudes in the middle atmosphere and influence both the mean and diurnally varying circulation and structure through thermal or density variations, direct transports of momentum and energy, and modulation of the fluxes due to gravity waves (Miyahara 1978a,b; Fritts and Vincent 1987; Fesen et al. 1991a,b; Wang and Fritts 1991; Forbes et al. 1991).

In the absence of direct measurements of wave energy and momentum fluxes and their divergence, the role of gravity wave forcing can best be assessed through measurement of wave amplitudes and anisotropy (or directionality), together with the scales and/or intrinsic frequencies of the observed motions. Most ground-based measurement systems provide information only on the vertical structure and observed frequencies of the motion field. Thus, intrinsic frequencies are uncertain in general, and horizontal scales are largely unknown except in a statistical sense. Some estimates for individual wave motions have been made using radars at several locations (Vincent and Reid 1983; Meek et al. 1985; Reid 1986; Reid and Vincent 1987; Manson and Meek 1988). More detailed information on the

Corresponding author address: Dr. David C. Fritts, Electrical and Computer Engineering Department, University of Colorado, Campus Box 425, Boulder, CO 80309-0425.

horizontal structure can be obtained, however, through the use of in situ or remote sensing aircraft measurement techniques or space shuttle–derived densities at greater heights (Nastrom and Gage 1985; Pfister et al. 1986; Fritts et al. 1989; Jasperson et al. 1990; Hostetler et al. 1991). Together with the associated wave amplitudes, such measurements provide a valuable view of the possible importance of wave forcing at heights well above those routinely observed by other systems.

We present in the following sections an analysis of the density fluctuations inferred at altitudes from 60 to 140 km with two accelerometer packages aboard several space shuttles during seven reentries into the earth's atmosphere. This effort extends our previous analysis of space shuttle density measurements (Fritts et al. 1989), which focused on fluctuations between 60 and 90 km, by applying more rigorous screening to the raw accelerometer data. The resulting density data are believed to be reliable to much greater heights and to provide a unique view of the potential for significant gravity wave forcing of the lower thermosphere. The flight reentry information, reentry cross sections, and data collection and analysis procedures are described in section 2. Fractional density data are displayed as functions of height and horizontal position and discussed in section 3. Section 4 presents the fractional density data in spectral form and examines the spectral changes with increasing height. Vertical profiles of fractional density variance computed to include and exclude, respectively, the contributions from wave structures with large vertical scales are examined in section 5. These data reveal a transition from significant wave amplitude growth with height at lower levels to a cessation of growth at large scales and apparent, more gradual growth at smaller scales at greater heights. Our conclusions are presented in section 6.

2. Data collection and analysis procedures

Data used for the analysis presented in this paper were obtained during seven space shuttle reentries, occurring primarily over the central Pacific at latitudes from ~10° to 30°N, with the one exception: a reentry from a 57° orbit over the North Pacific. The reentry dates and 90-km geographic locations are listed for reference in Table 1. The reentry track for each descent for altitudes from 140 to 60 km is shown in Fig. 1.

Densities during each reentry were inferred using two instruments aboard the space shuttles *Challenger* and *Columbia*. The inertial Measurement Unit (IMU) used for onboard navigation and guidance is a three-axis accelerometer providing sensitivity primarily at lower altitudes. The High Resolution Accelerometer Package (HIRAP), of greater relevance to our analysis, provides measurements at greater heights at a data rate of 174 Hz and with a sensitivity of 2–10 ($\times 10^{-6}$ g). Used together with an estimate of the aerodynamic drag coefficient obtained from pressure sensors aboard one shuttle and information on the shuttle velocity and area/mass ratio, the accelerometer data permit computation of the atmospheric density during each sample interval. The resulting density estimates were then averaged for 1 s after removal of values obtained during thrust events or control surface motions. This yielded density estimates at a horizontal spacing ranging from ~7.5 to 5 km at altitudes of 140 and 60 km, respectively. For ease of presentation, these densities were normalized by the *U.S. Standard Atmosphere, 1976*. However, the assumed model atmosphere has no influence on the inferred wave structures. Additional information on the accelerometer packages and the computation of atmospheric density is provided by Blanchard and Rutherford (1985) and Blanchard and Buck (1986).

TABLE 1. Reentry data and 90-km location for shuttle flights included in this analysis.

Reentry	Date	Lat (90 km) (°N)	Long (90 km) (°W)
6	9 April 1983	17	174
7	24 June 1983	27	181
8	5 September 1983	24	178
9	8 December 1983	56	198
11	11 February 1984	28	144
13	13 April 1984	16	177
32	18 January 1986	25	182

Density measurements with the onboard accelerometers were obtained along slanted reentry paths determined to allow for shuttle deceleration without excessive heating. As a result, the reentry paths were steeply inclined until the shuttles encountered sufficient densities to provide adequate drag, at which point the reentry paths flattened to dissipate kinetic energy prior to further descent. This transition normally occurred near 75 km, with a descent rate of ~1 km vertical/50 km horizontal at greater heights and a rate of ~1 km vertical/200 km horizontal at lower levels. The reentry path and velocity profile for shuttle flight 11 are representative and are shown in Figs. 2 and 3 for reference.

Density measurements made along these slanted reentry paths provide sensitivity simultaneously to horizontal and vertical structure of the atmosphere. It was argued by Fritts et al. (1989) that the more nearly horizontal tracks below ~78 km represented nearly horizontal sampling of the density field because reentry path slopes were typically less than characteristic phase slopes of the gravity waves accounting for the density fluctuations. This is not necessarily the case at greater heights, however, where reentry path slopes are comparable to or steeper than the phase slopes of the dominant gravity wave and tidal motions. This introduces an ambiguity in the estimation of horizontal scales in addition to the uncertainty implied by lack of knowl-

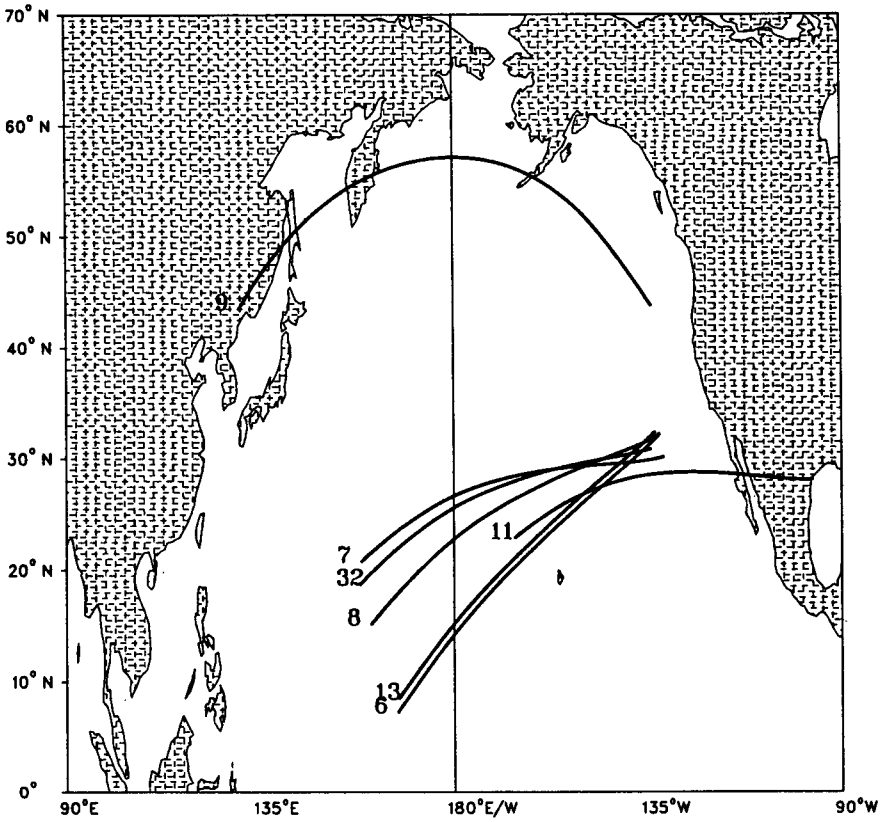

FIG. 1. Geographic locations of reentry tracks for the seven shuttle flights used in this analysis between 140 and 60 km.

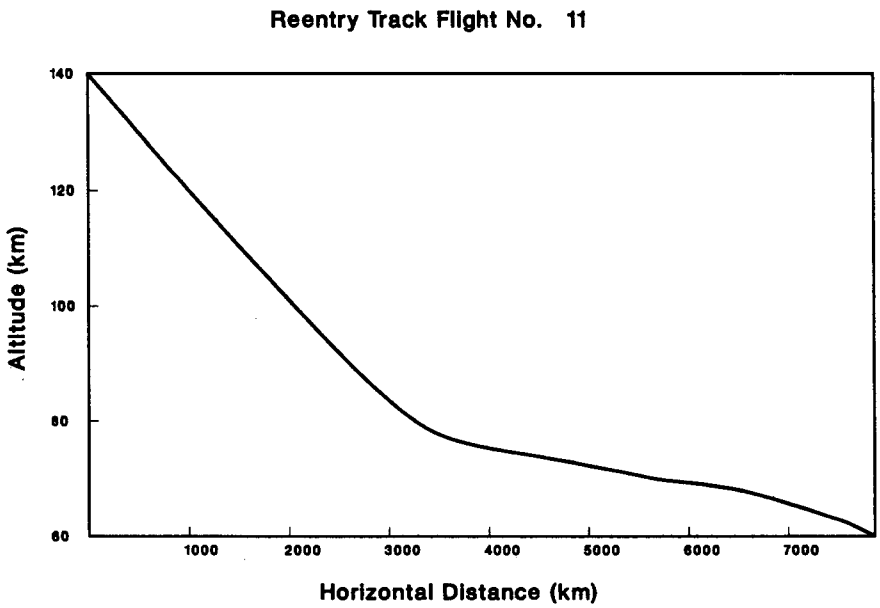

FIG. 2. Height profile of reentry track for shuttle flight 11. The descent rate is approximately four times greater above than below ~75 km.

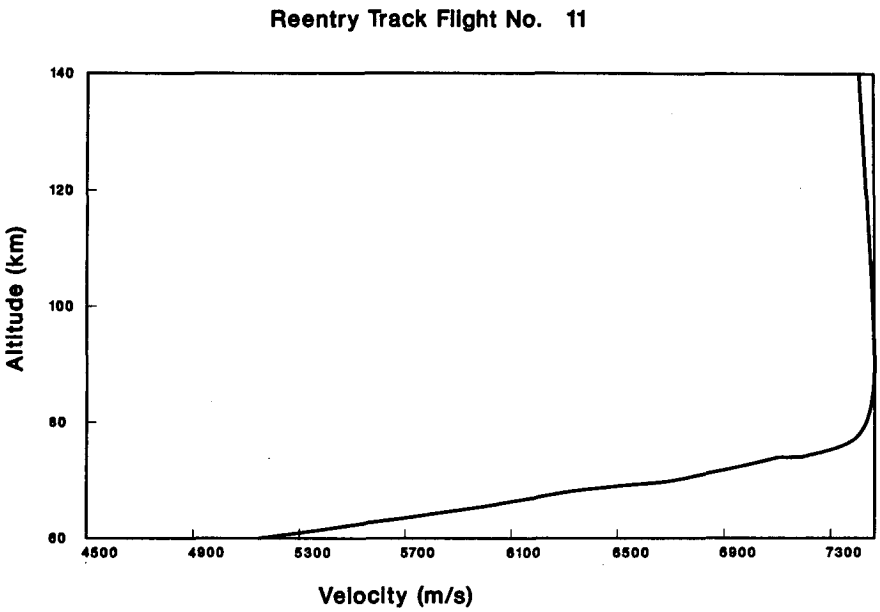

FIG. 3. Reentry velocity versus altitude for shuttle flight 11. Note that deceleration occurs primarily along the nearly horizontal segment between ~80 and 60 km.

edge of the direction of wave propagation relative to shuttle motion.

The relative influences of horizontal and vertical structures on the slant wavelengths inferred during reentry may be evaluated by writing the wavenumber vector $\mathbf{k} = (k, l, m)$, with $\hat{x}$, $\hat{y}$, and $\hat{z}$ east, north, and up, in a frame with $\hat{x}'$, $\hat{y}'$, and $\hat{z}'$ along, horizontally normal, and upward and normal to the flight track. In this "shuttle" coordinate system, the apparent wavenumber components are

$$k' = \mathbf{k} \cdot \hat{x}' = k \cos\phi \cos\psi + l \cos\phi \sin\psi - m \sin\phi, \quad (1)$$

$$l' = \mathbf{k} \cdot \hat{y}' = -k \cos\phi \sin\psi + l \cos\phi \cos\psi - m \sin\phi, \quad (2)$$

and

$$m' = \mathbf{k} \cdot \hat{z}' = k \sin\phi \cos\psi + l \sin\phi \sin\psi + m \cos\phi, \quad (3)$$

where ϕ is the descent angle and ψ is the angle of the flight track north of east.

Now noting that typical (hydrostatic) gravity wave and tidal motions have $k^2, l^2 \ll m^2$ and that the descent angle ϕ (relative to the horizontal) is at most ~0.02 rad, the wavenumber along the reentry track may be written

$$k' \approx k \cos\psi + l \sin\psi - m\phi. \quad (4)$$

To an excellent approximation, then, apparent horizontal wavenumbers may be strongly biased when k/m and $l/m \approx \omega/N \approx \theta$ are $\sim\phi$ (or alternatively, for low-frequency wave motions), where ω and N are the intrinsic and buoyancy frequencies and θ is the angle between the wave phase front and the horizontal. This is particularly true above ~75 km, where the descent angle is steeper. Horizontal wavenumber estimates are influenced to a lesser degree by vertical wave structure at higher intrinsic frequencies because m is more nearly comparable to k and l and thus contributes only a small amount to k'. In this case, however, k' may vary from the horizontal wavenumber in the direction of wave propagation to infinity. Thus, it is important to recognize that horizontal wavenumber spectra computed using space shuttle density data, particularly above ~75 km, are at best only suggestive of the true horizontal wave field structure. With sufficient randomness of wave propagation direction, however, and especially at higher frequencies and smaller horizontal scales, inferences about relative spectral amplitudes and slopes at different heights should provide valid statistical views of the mean wave field and its changes with height.

Slant wavenumber spectra of fractional densities were computed for altitude ranges of 60–80, 80–110, and 110–140 km to evaluate spectral amplitude and shape changes with height, to assess which horizontal scales contributed preferentially to growth, and to determine the sensitivity to small-scale motions in each range. Spectra were computed assuming an average data spacing in the lower altitude range of 6 km, where the space shuttle velocity decreased from ~7.5 to 5 km s^{-1}, and with a spacing of 7.5 km in the upper ranges, where the velocity was more nearly constant.

A Hamming window was used to avoid aliasing of variance to higher wavenumbers and the resulting spectra were compensated to preserve the total spectral variance. Mean spectra were then assembled from the individual spectra in each height range.

Profiles of wave variance were computed in two ways to include and exclude the variance due to large-scale motions. The intent was to evaluate separately the contributions by gravity waves and tidal motions to the overall fractional density variance at each height. Total variance in height intervals of 5 and 10 km were computed from the departures of the measured densities from the *U.S. Standard Atmosphere.* Variance estimates reflecting more nearly those contributions only from gravity waves were obtained for each height interval by first removing the mean and linear trend of the density fluctuations about the *U.S. Standard Atmosphere.* This effectively removed tidal variance because tidal wavelengths are substantially larger, both in the vertical and horizontal, than the intervals over which these variances were computed.

3. Vertical and horizontal profiles of fractional densities

a. Fractional density variations with height

Vertical profiles of fractional densities obtained for the seven space shuttle reentries at altitudes from 60 to 140 km are shown in Fig. 4. The spacing between profiles represents a fractional density fluctuation of 100%. These profiles suggest significant increases in wave activity and fractional density variance at large and small scales with increasing height. Because this presentation of the density fluctuations masks the variations occurring at lower altitudes, however, these profiles are shown in Fig. 5 for the three altitude ranges defined above with different amplitude scalings and with a linear trend removed in each case. Note in both Figs. 4 and 5 that the higher data density with height between 60 and 80 km resulted from the same sampling rate of the density field along a reentry path that descended approximately four times more slowly than at greater heights.

The profiles in Fig. 5 also reveal a changing character of the density fluctuations with height. There was little evidence of large-scale motions in the lower altitude range and amplitudes were typically ~1%–5% relative to the standard atmosphere density. Note especially that the structures appearing with large amplitudes and small vertical scales in Fig. 5 almost certainly correspond to horizontal variations rather than vertical variations of density. The reason is that fractional density fluctuations are proportional to horizontal velocity fluctuations and thus have their vertical gradients limited by instability processes (Smith et al. 1987; Fritts et al. 1989).

The profiles between 80 and 110 km suggest slight growth of these smaller-scale motions but a significant increase in the amplitudes of larger vertical scales relative to the lower altitude range. The dominant structures here, assuming for the moment that these were primarily vertical and not horizontal variations of den-

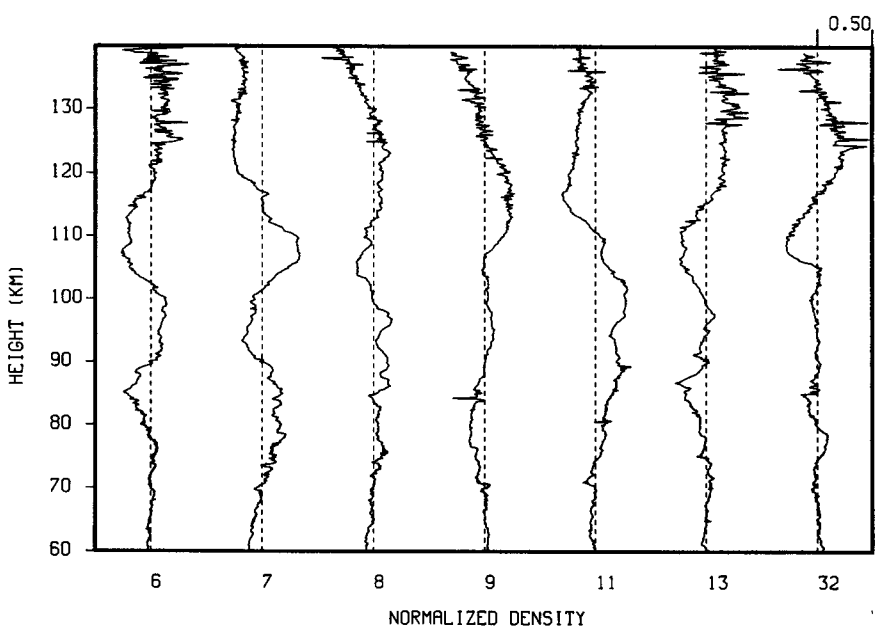

FIG. 4. Fractional densities versus altitude from 60 to 140 km for the seven reentries used in this analysis. The 50% fluctuation amplitude is shown at the upper right.

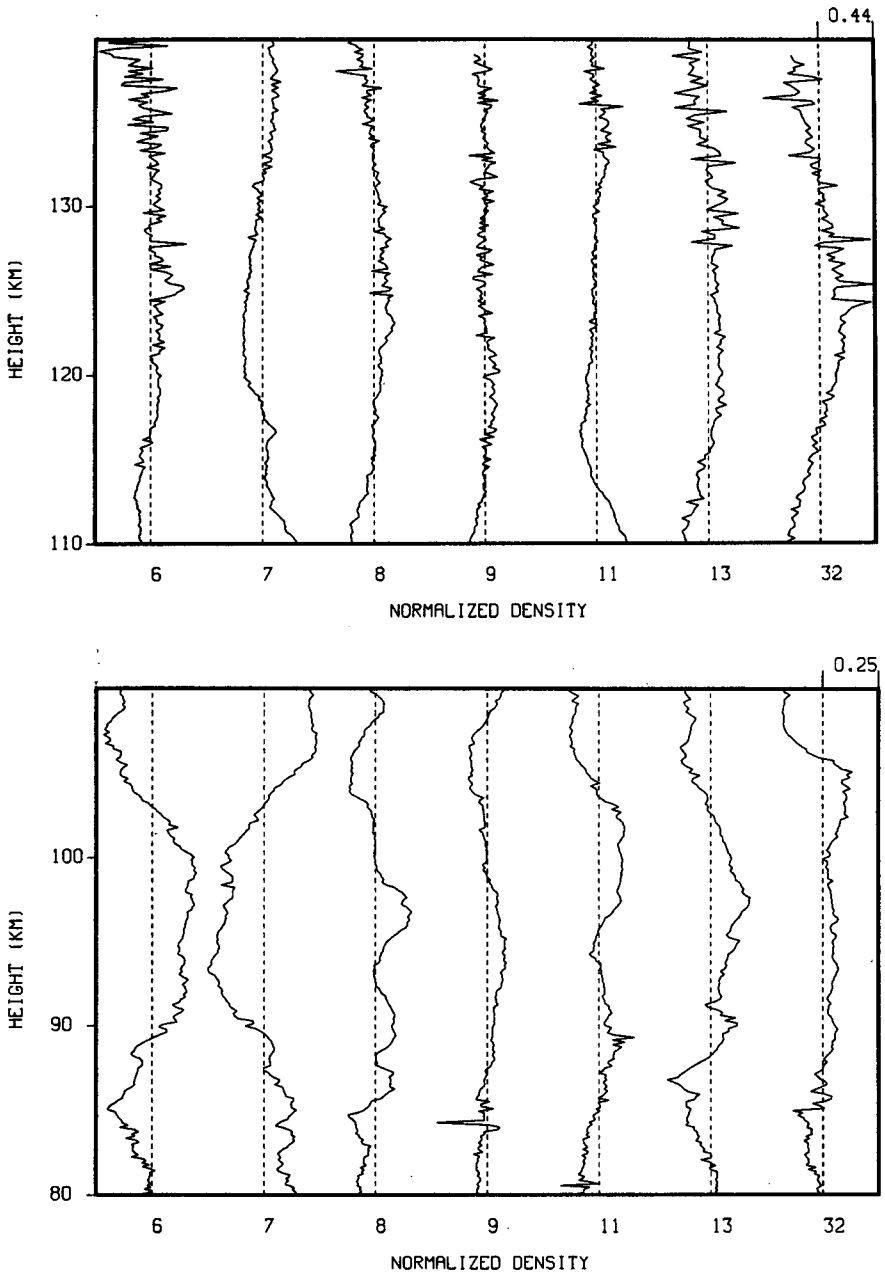

FIG. 5. As in Fig. 4 but for altitude ranges of (a) 110–140, (b) 80–110, and (c) 60–80 km. Note the different amplitude scalings at the upper right in each case.

sity, had vertical wavelengths of ~25 km and achieved amplitudes of ~20%–30%, in reasonable agreement with tidal theory and observations of very large tidal amplitudes in the velocity field at these heights over Hawaii (Forbes et al. 1991; Fritts and Isler 1992). Tidal density and velocity fluctuations are not directly related, however, due to varying latitudinal structure and because other processes, such as dissipation, may also influence tidal fluctuations (Forbes and Vincent 1989). Assuming these fluctuations to be tidal in nature, the shuttle descent path would span a vertical wavelength in only ~1250 km horizontally, representing only a small fraction of the diurnal or semidiurnal horizontal wavelength at this latitude. The ubiquity of density variations with these characteristics and the independent observations of such tidal structures at this central

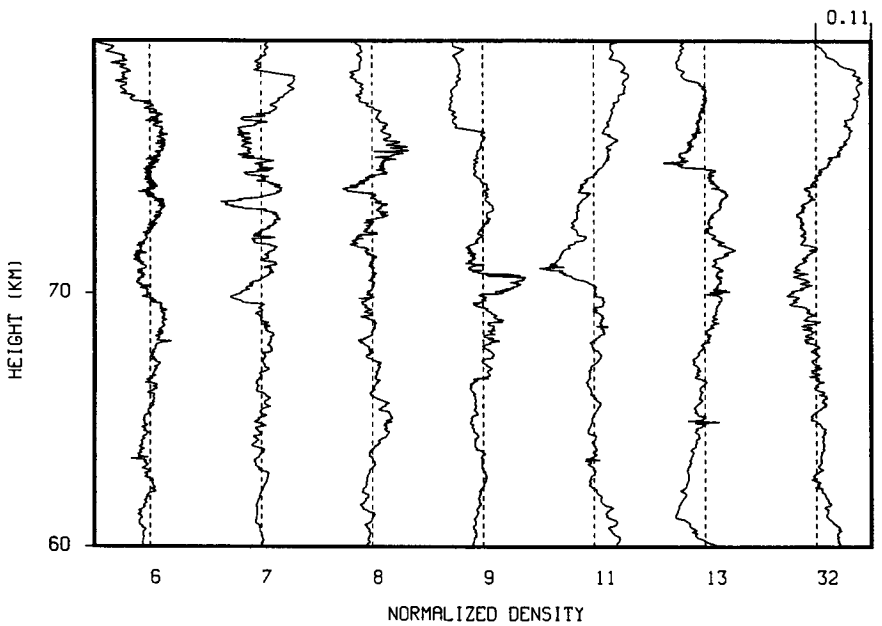

FIG. 5. (*Continued*)

Pacific location suggest strongly that these motions are tidal in nature.

Smaller-scale features in the 80–110-km altitude range, like those at lower levels, were most likely associated with horizontal variations of density and exhibit amplitudes of ~2%–10%. Vertical scales at these heights do not appear as small because of the larger vertical sampling interval due to the more rapid descent above ~80 km. Present in this and the lower altitude range were density variations with large amplitudes occurring very near the Nyquist wavenumber (a wavelength of ~12–15 km). Such features (see flight 9 near 71 and 84 km, flight 11 near 71 and 81 km, and flight 13 near 65 km, for examples), assuming they were due to gravity waves, must represent wave motions with large horizontal velocity fluctuations, large vertical scales, and small horizontal scales. Those features containing a number of cycles, in particular, appear well defined and coherent and were likely isolated, large-amplitude wave packets that may have large statistical influences in the mesosphere and thermosphere.

For gravity waves, the horizontal velocity associated with a particular density fluctuation can be estimated following Fritts et al. (1989) as

$$\rho'/\bar{\rho} \approx Nu'/g, \tag{5}$$

assuming that the motions are nearly hydrostatic and not influenced by rotation. For a value of $N \sim 0.015$ s^{-1} appropriate for the mesosphere, this implies a velocity fluctuation of ~6 m s^{-1} for each 1% density variation. Thus, density variations of 2%–10% correspond to horizontal velocities of ~12–60 m s^{-1}. Likewise, saturation and/or wave–wave interaction processes appear to limit the vertical shears within the wave field to values of $u'_z \sim N$ (Dewan and Good 1986; Smith et al. 1987; Hines 1991), implying minimum vertical scales for these density fluctuations of $\lambda_z = 2\pi/m \sim 6$–30 km. Given the vertical scales implied by the presentation in Figs. 4 and 5 of substantially less than 1 km, these fluctuations can only be due to horizontal variations of density.

Density variations observed in the upper-altitude range exhibit large-scale features with similar scales and amplitudes to those seen in the intermediate range. Also present are indications that small-scale structures continue to increase with height. Reentries 6, 13, and 32, in particular, contain small-scale density variations of ~20%–30% at heights above ~125 km. It will be seen below, however, that a portion of this increased variance at small scales may be due to a decreasing sensitivity to very small density fluctuations at these high altitudes.

b. *Fractional density variations with horizontal distance*

Fractional densities as a function of horizontal position are displayed for each altitude range in Fig. 6, again with the mean and linear trend removed from each profile and with different amplitude scalings for each range. In contrast to the discussion above, where the observed scales were only realistic for the large-scale components of the wave field, the fractional den-

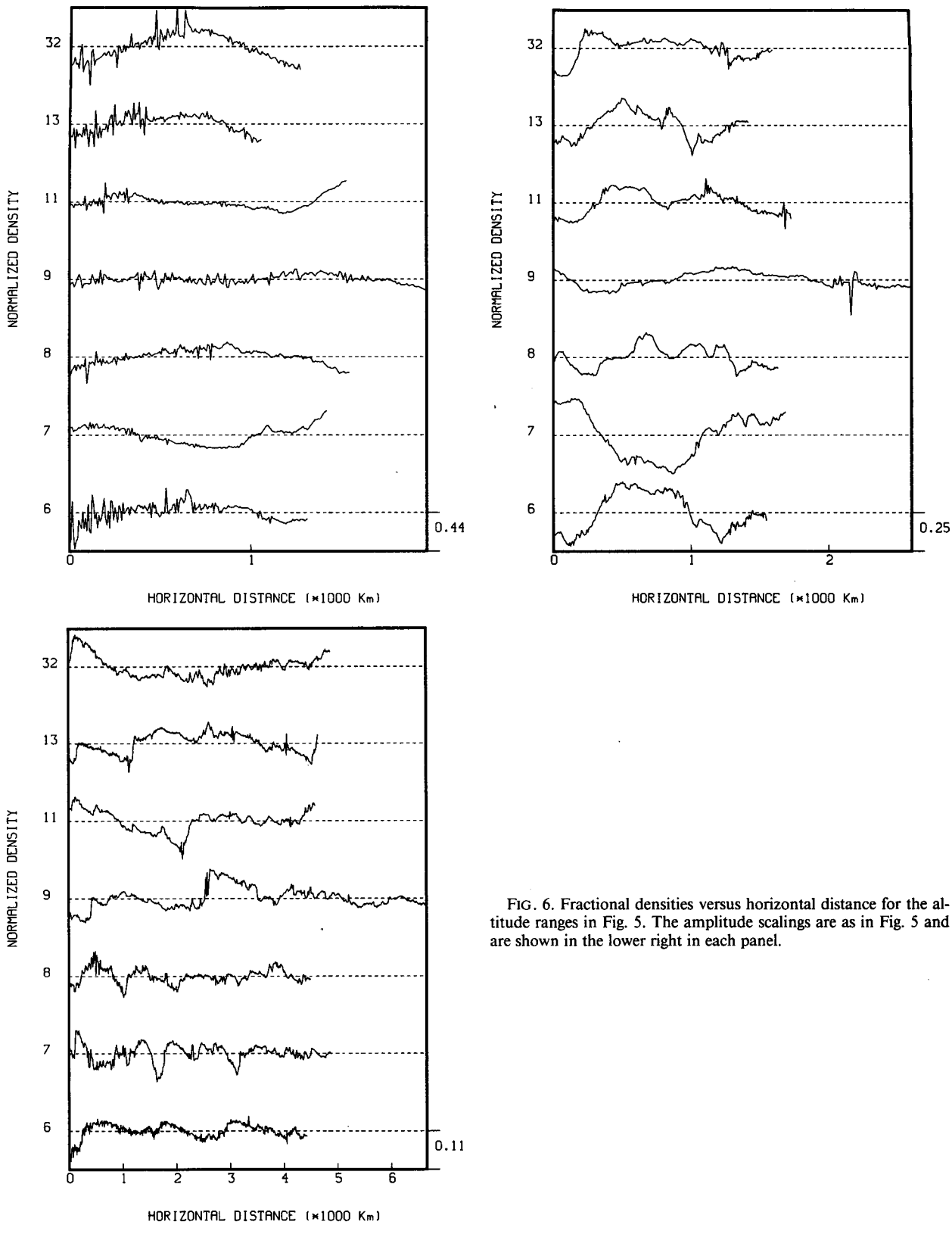

FIG. 6. Fractional densities versus horizontal distance for the altitude ranges in Fig. 5. The amplitude scalings are as in Fig. 5 and are shown in the lower right in each panel.

sities displayed in this manner now provide more reliable information on the spatial structure of small-scale motions with higher intrinsic frequencies. The different lengths of the data segments in each profile simply reflect the slight variations in the angle of the reentry path for each flight. Note, for example, that the upper (and deeper) altitude ranges were transitted in only ~1500 km horizontally while the data segments for the shallower, lower ranges each extended for ~4000–5000 km horizontally. The anomaly was reentry 9, which encountered significant small-scale structure in the upper- and lower-altitude ranges and descended at a more gradual rate to provide slower deceleration.

These density profiles reinforce the statements made above about the apparent small horizontal scales and large wave amplitudes occurring at specific heights. The profiles for reentry 9 provide the clearest examples, with apparent density jumps or large oscillations at the Nyquist wavenumber occurring at several locations. Other reentries were not immune to large and/or rapid density changes, however. Isolated, large-amplitude, and small-scale features were encountered at many locations, while several profiles, most notably reentry 6, exhibited sustained activity at very small horizontal scales for large distances.

Also noted in the density data presented in this manner are the large increases in the amplitudes of the large-scale features from the lower to the intermediate altitude range and the growth of amplitudes at very small horizontal scales in the upper altitude range. It is not easy to compare spatial scales from the lower to the upper altitude ranges because of the very different horizontal scales needed to present each. Yet it is evident that significant fluctuations occur close to the Nyquist wavenumber at virtually all heights. Thus, gravity waves with relatively small horizontal scales and large amplitudes (and correspondingly large momentum fluxes) must be playing a major role in forcing the circulation and structure of the lower thermosphere.

4. Slant wavenumber spectra of fractional densities

We now turn to an assessment of the spectral characteristics of the fractional density fluctuations as a function of horizontal position. Mean slant wavenumber spectra are presented in both standard and variance content forms for each altitude range in Fig. 7. As noted above, these spectra likely provide an accurate view of the variances at higher slant wavenumbers, for which vertical wave structure introduces less potential error, but bias the variance assumed to be due to tidal motions to very much larger apparent (horizontal) wavenumbers than they have in reality.

The slant wavenumber spectra in standard form for each altitude range (left panels in Fig. 7) reveal structure at intermediate wavenumbers that follows approximately a -2 power law. The largest scales in the upper altitude ranges exhibit enhanced variance due to aliasing of tidal variance into this spectral range (15–30 km), while spectral slopes depart increasingly from an approximately -2 slope at large wavenumbers with increasing height. This transition to a flatter mean spectrum in each altitude range suggests either 1) an increasing noise floor due to increasing measurement uncertainties with increasing height or 2) a preferential vertical propagation of wave motions with very high intrinsic frequencies. We will consider each possibility in turn.

We assume first that the change in spectral character at large slant wavenumbers is caused by measurement uncertainties implying a white (i.e., flat) noise spectrum. In the lower altitude range, this noise floor appears to occur near a spectral variance of $\sim 10^{-4}$ km cyc^{-1} (kilometers per cycle) and to influence strongly scales less than ~25 km. This noise floor appears to increase in the intermediate and upper altitude ranges to $\sim 10^{-3}$ and 10^{-2} km cyc^{-1} and to influence strongly scales smaller than ~50 and 100 km, respectively. The impact on scale sensitivity in the intermediate and upper altitude ranges would be even more severe if the variance contributed by the wave spectrum did not also increase with height. The apparent enhanced spectral noise floors and decreased sensitivity at upper levels suggest that we must be careful in inferring properties of the small-scale wave field at these heights. In particular, the presence and rapid growth of such motions above ~125 km must be carefully questioned.

The second option, that the slant wavenumber spectra are enhanced at large wavenumbers due to the enhanced vertical propagation of motions with high intrinsic frequencies, is certainly a possibility. Indeed, we expect motions with higher intrinsic frequencies and more rapid vertical propagation to more effectively avoid increasing turbulent and/or molecular dissipation at greater altitudes. However, the character of the motion field at lower altitudes suggests that the frequency and wavenumber spectra are approximately separable (Fritts and Chou 1987). This suggests that gravity waves at all high slant wavenumbers should have statistically similar distributions with intrinsic frequency and that there should be no preference for enhanced vertical propagation only at very small spatial scales. Thus, we conclude that the increasing noise floor with increasing altitude is the more likely explanation of the changes in spectral shape with height.

Another view of the spectral character of the fractional density fluctuations in each altitude range is provided by the variance content form of the slant wavenumber spectrum. This form weights each spectrum by slant wavenumber $[k'E(k')]$ to show more clearly the wavenumbers contributing most to the total spectral variance. Inspection shows that the noise floor in the lower-altitude range contributes very little to the overall spectral variance, but that this contribution increases significantly with increasing altitude. The con-

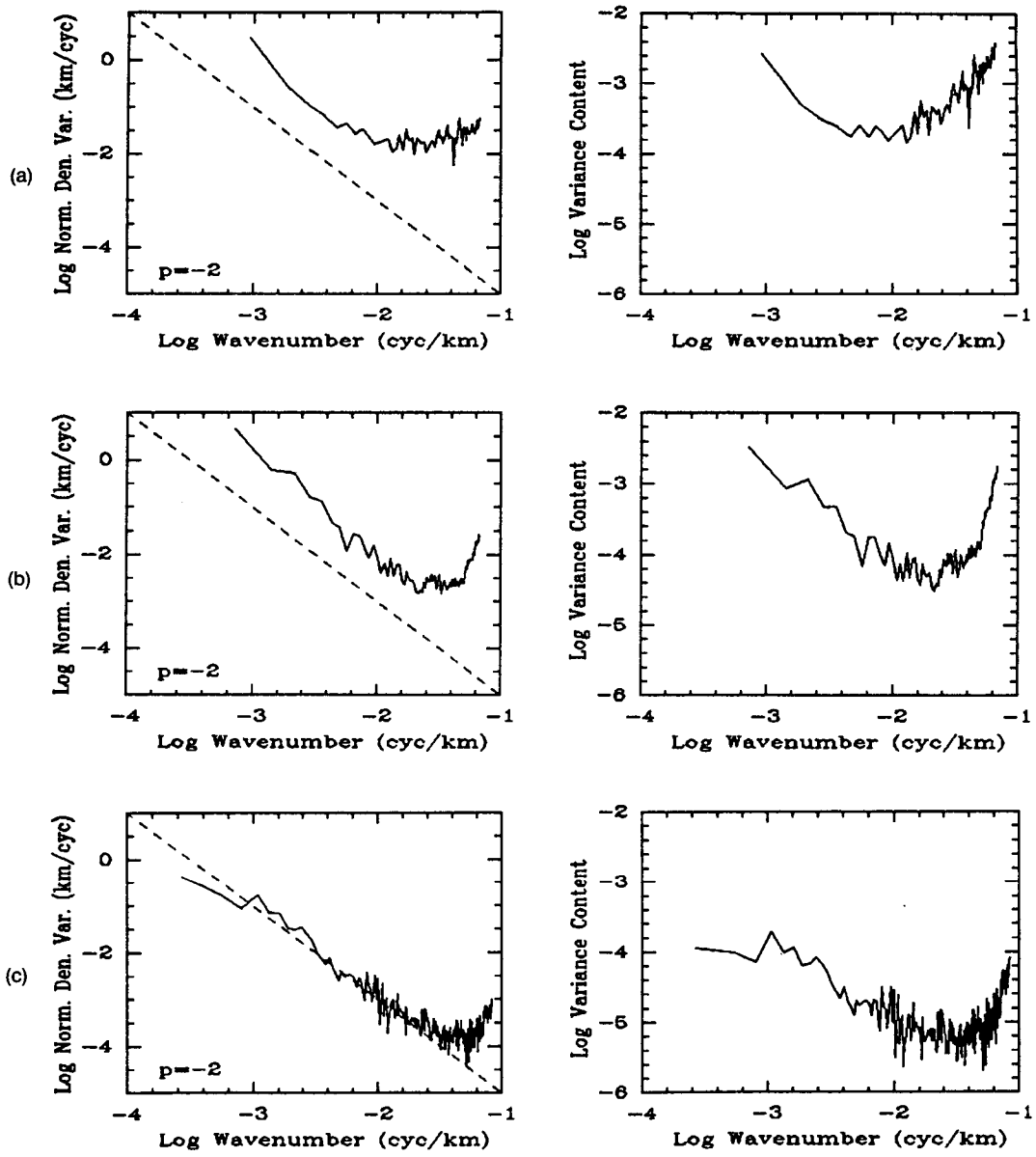

FIG. 7. Slant wavenumber spectrum of fractional density variance in standard (left panels) and variance content (right panels) forms for the altitude ranges in Fig. 5. The dashed lines in the left panels show a slope of −2 for reference. Note the increasing noise floor with increasing altitude and the different Nyquist wavenumbers below and above 80 km.

tribution remains nearly negligible, relative to tidal and larger-scale gravity wave terms, in the intermediate altitude range. In the upper range, however, this noise variance appears to make up an appreciable fraction of the total and must be accounted for in assessing the changes in wave variance with increasing altitude.

5. Vertical profiles of fractional density variance

Profiles of fractional density variance computed in 5-km and 10-km segments to reflect large- and small-scale motions are presented in Figs. 8 and 9. In each case, the variance profiles obtained for individual reentries are shown with dotted lines and the mean profile is shown with a solid line. Referring first to the large-scale variance profiles that include tidal contributions, we note at lower altitudes an increase consistent with that reported previously by Fritts et al. (1989) for small-scale motions between 60 and 90 km. The variance in this range exhibits a growth with altitude that is approximately exponential with a scale height of ~12–

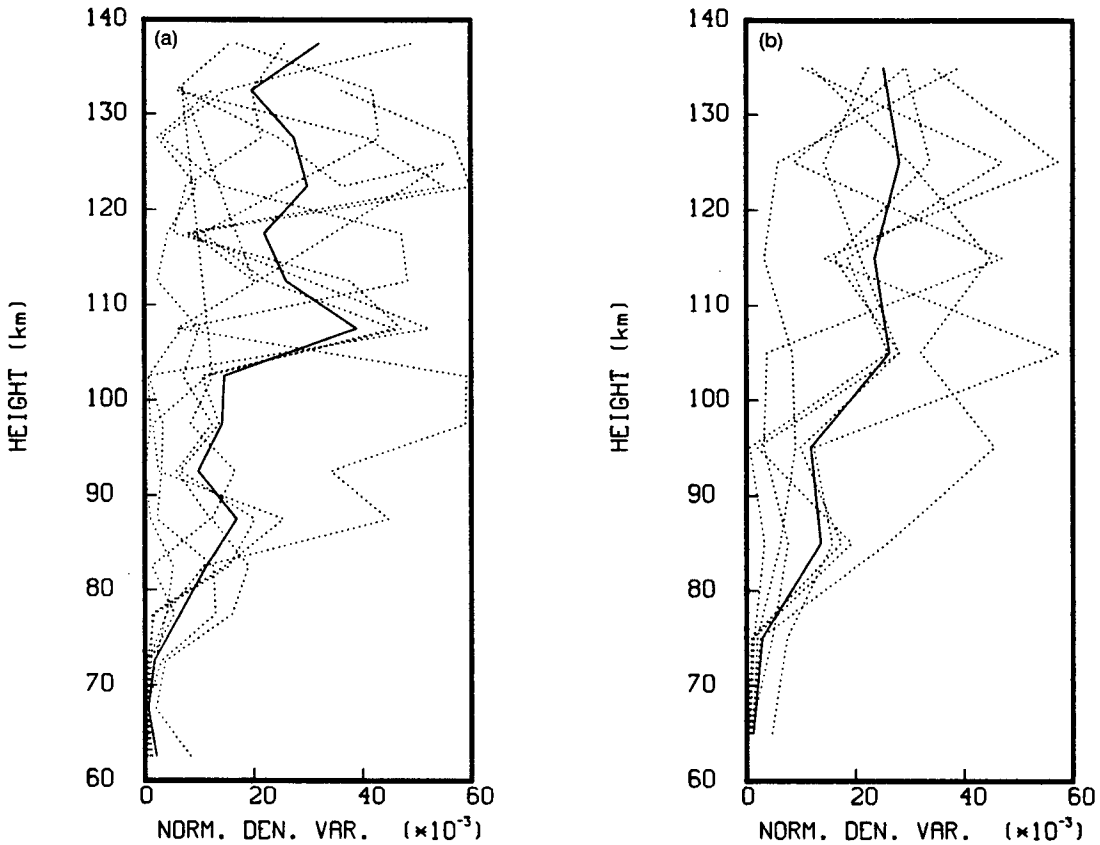

FIG. 8. Variance profiles computed in (a) 5- and (b) 10-km altitude intervals reflecting all departures from the *U.S. Standard Atmosphere, 1976*. Dotted and solid lines show individual and mean profiles.

15 km and consistent with that noted throughout the lower atmosphere (Balsley and Carter 1982; Balsley and Garello 1985; Fritts 1989). At greater heights, there is a clear tendency for the growth of wave variance to slow and finally cease, due presumably to the large increase in molecular dissipation encountered as wave motions enter the lower thermosphere. Not surprisingly, this cessation of wave amplitude growth coincides closely with the altitude of the turbopause and a transition from wave amplitude–limiting saturation or interaction processes to diffusive processes. The 5- and 10-km variance profiles also provide a consistent view of the total variance because both were computed without exclusion of variance at large vertical scales.

Referring now to the variance profiles in Fig. 9, we note substantially less total variance than seen in Fig. 8 due to the exclusion of variance at scales larger than 5 and 10 km, respectively. Variances observed below 90 km are essentially identical to those presented by Fritts et al. (1989), while at greater heights the gravity wave variances parallel to a large degree the large-scale variances representing primarily tidal contributions (see Fig. 8). Variances above 80 km for 5- and 10-km segments include horizontal scales less than ~250 and 500 km, respectively. Given that the wave spectrum at these heights contains significant variance at such scales, it is not surprising that the 10-km variances are ~2–3 times larger than those in 5-km intervals up to ~120 km. For the same reason, these variance profiles likely do not reflect all the variance that should be associated with the gravity wave spectrum at these heights.

Like the large-scale variance profiles, the variances computed in 5- and 10-km height intervals exhibit a slowing or cessation of growth above ~100 km suggesting, as noted above, an increasingly important role for molecular rather than turbulent dissipation (i.e., the turbopause) of wave motions propagating into the lower thermosphere. The apparent growth in small-scale variance above ~120 km is also likely only an artifact of the increasing uncertainty in density determinations due to an exponentially decreasing density at greater altitudes, as discussed above in connection with the spectral results. Correction of these profiles to remove the artificial increase at upper levels does not influence appreciably the large-scale variance profiles

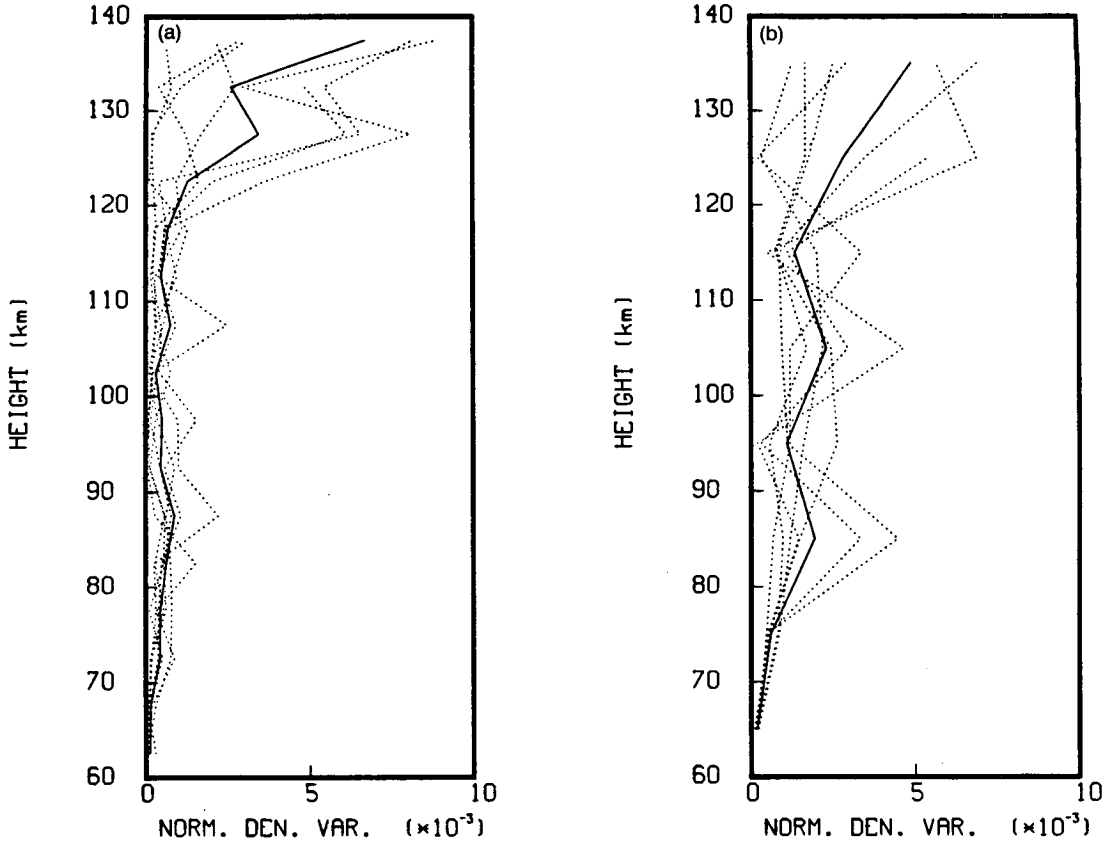

FIG. 9. As in Fig. 8 but for small-scale departures from the *U.S. Standard Atmosphere, 1976*. See text for details.

because the correction is less than 1/10 of the total variance at the highest altitudes. An important final point is that even without the apparently spurious increase in small-scale wave variance above ~120 km, there is ample wave activity present at sufficiently small horizontal scales to have a dramatic influence on the circulation and thermal structure of the lower thermosphere.

6. Conclusions

We have presented an analysis of density measurements obtained during seven space shuttle reentries into the atmosphere at altitudes from 60 to 140 km. These results extend those previously reported by Fritts et al. (1989) and provide an indication of the level of gravity wave and tidal activity in the lower thermosphere away from major landmasses. The dominant scales and amplitudes of the wave structures present in the data, as well as their variations with altitude, were assessed. Large-scale structures were attributed to tidal motions with vertical wavelengths of ~25 km and horizontal wavelengths of thousands of kilometers. These motions exhibited a clear growth with height up to ~110 km, above which amplitude growth ceased. Smaller-scale features in the density profiles were attributed to gravity waves at horizontal scales ranging from ~10 to 1000 km. The amplitudes of small-scale features suggested vertical scales of ~6 to 30 km and implied that the small-scale features of the fractional density profiles corresponded, in reality, to horizontal rather than vertical variations of density. Like the large-scale structures, gravity wave scales were observed to increase in amplitude up to ~100 km.

Slant wavenumber spectra revealed an increase in both the wave and noise variance with altitude, causing the density measurements to be less sensitive to small spatial scales at greater heights. The noise floor was estimated to begin at horizontal scales of ~25, 50, and 100 km for the three altitude ranges of 60–80, 80–110, and 110–140 km. Spectral variance estimates nevertheless confirmed the growth of gravity wave amplitudes up to ~100 km and the maintenance of approximately constant amplitudes at greater heights. Together, these results provide substantial evidence that gravity waves as well as tidal motions provide strong forcing of the circulation and structure of the lower thermosphere.

Acknowledgments. This research was supported by the Air Force Office of Scientific Research (AFSC) un-

der Grant AFOSR-91-0026 and by the SDIO/IST and managed by the Office of Naval Research under Contract N00014-90-J-1271.

REFERENCES

Balsley, B. B., and D. A. Carter, 1982: The spectrum of atmospheric velocity fluctuations at 8 and 86 km. *Geophys. Res. Lett.*, **9**, 465–468.

——, and R. Garello, 1985: The kinetic energy density in the troposphere, stratosphere and mesosphere: A preliminary study using the Poker Flat radar in Alaska. *Radio Sci.*, **20**, 1355–1362.

Blanchard, R. C., and G. M. Buck, 1986: Rarefied-flow aerodynamics and thermosphere structure from shuttle flight measurements. *J. Spacecr. Rockets*, **23**, 18–24.

——, and J. F. Rutherford, 1985: Shuttle orbiter high resolution accelerometer package experiment: Preliminary flight results. *J. Spacecr. Rockets*, **22**, 474–480.

Blix, T. A., E. V. Thrane, D. C. Fritts, U. von Zahn, F.-J. Lübken, W. Hillert, S. P. Blood, J. D. Mitchell, G. A. Kokin, and S. V. Pakhomov, 1990: Small-scale structure observed *in-situ* during MAC/EPSILON. *J. Atmos. Terr. Phys.*, **52**, 835–854.

Dewan, E. M., and R. E. Good, 1986: Saturation and the "universal" spectrum for vertical profiles of horizontal scalar winds in the atmosphere. *J. Geophys. Res.*, **91**, 2742–2748.

Dunkerton, T. J., 1989: Theory of internal gravity wave saturation. *Pure Appl. Geophys.*, **130**, 373–397.

Fesen, C. G., R. G. Roble, and E. C. Ridley, 1991a: Thermospheric tides at equinox: Simulations with coupled composition and auroral forcing. 1: diurnal component. *J. Geophys. Res.*, **96**, 3647–3662.

——, ——, and ——, 1991b: Thermospheric tides at equinox: Simulations with coupled composition and auroral forcing. 2: semidiurnal component. *J. Geophys. Res.*, **96**, 3663–3678.

Forbes, J. M., and R. A. Vincent, 1989: Effects of mean winds and dissipation of the diurnal propagating tide: An analytic approach. *Planet. Space Sci.*, **37**, 197–209.

——, R. G. Roble, and C. G. Fesen, 1993: Acceleration, heating, and compositional mixing of the thermosphere due to upward-propagating tides. *J. Geophys. Res.*, **96**, in press.

Fritts, D. C., 1984: Gravity wave saturation in the middle atmosphere: A review of theory and observations. *Rev. Geophys. Space Phys.*, **22**, 275–308.

——, 1989: A review of gravity wave saturation processes, effects, and variability in the middle atmosphere. *Pure Appl. Geophys.*, **130**, 343–371.

——, and H.-G. Chou, 1987: An investigation of the vertical wavenumber and frequency spectra of gravity wave motions in the lower stratosphere. *J. Atmos. Sci.*, **44**, 3610–3624.

——, and R. A. Vincent, 1987: Mesospheric momentum flux studies at Adelaide, Australia: Observations and a gravity wave/tidal interaction model. *J. Atmos. Sci.*, **44**, 605–619.

——, and L. Yuan, 1989: Measurement of momentum fluxes near the summer mesopause at Poker Flat, Alaska. *J. Atmos. Sci.*, **46**, 2569–2579.

——, and J. R. Isler, 1992: First observations of mesospheric dynamics with a partial reflection radar in Hawaii (22°N, 160°W). *Geophys. Res. Lett.*, **19**, 409–412.

——, R. C. Blanchard, and L. Coy, 1989: Gravity wave structure between 60 and 90 km inferred from space shuttle reentry data. *J. Atmos. Sci.*, **46**, 423–434.

Garcia, R. R., 1989: Dynamics, radiation, and photochemistry in the mesosphere: Implications for the formation of noctilucent clouds. *J. Geophys. Res.*, **94**, 14 605–14 615.

Hines, C. O., 1991: The saturation of gravity waves in the middle atmosphere. Part II: Development of Doppler-spread theory. *J. Atmos. Sci.*, **48**, 1360–1379.

Hostetler, C. A., C. S. Gardner, R. A. Vincent, and D. Lesicar, 1991: Spectra of gravity wave density and wind perturbations observed during ALOHA-90 on the 25 March flight between Maui and Christmas Island. *Geophys. Res. Lett.*, **18**, 1325–1328.

Jasperson, W. H., G. D. Nastrom, and D. C. Fritts, 1990: Further study of terrain effects on the mesoscale spectrum of atmospheric motions. *J. Atmos. Sci.*, **47**, 979–987.

Manson, A. H., and C. E. Meek, 1988: Gravity wave propagation characteristics (60–120 km) as determined by the Saskatoon MF radar (Gravnet) system: 1983–1985 at 52°N. *J. Atmos. Sci.*, **45**, 932–946.

McIntyre, M. E., 1989: On dynamics and transport near the polar mesopause in summer. *J. Geophys. Res.*, **94**, 14 617–14 628.

Meek, C. E., I. M. Reid, and A. H. Manson, 1985: Observations of mesospheric wind velocities. I: Gravity wave horizontal scales and phase velocities determined from spaced wind observations. *Radio Sci.*, **20**, 1373–1382.

Miyahara, S., 1978a: Zonal mean winds induced by vertically propagating atmospheric tidal waves in the lower thermosphere. Part I: *J. Meteor. Soc. Japan*, **56**, 86–97.

——, 1978b: Zonal mean winds induced by vertically propagating atmospheric tidal waves in the lower thermosphere. Part II: *J. Meteor. Soc. Japan*, **56**, 548–558.

Nastrom, G. D., and K. S. Gage, 1985: A climatology of atmospheric wavenumber spectra of wind and temperature observed by commercial aircraft. *J. Atmos. Sci.*, **42**, 950–960.

Pfister, L., W. Starr, R. Craig, M. Loewenstein, and M. Legg, 1986: Small-scale motions observed by aircraft in the lower tropical stratosphere: Evidence for mixing and its relationship to large-scale flows. *J. Atmos. Sci.*, **43**, 3210–3225.

Reid, I. M., 1986: Gravity wave motions in the upper middle atmosphere (60–110 km). *J. Atmos. Terr. Phys.*, **48**, 1057–1072.

——, and R. A. Vincent, 1983: HF Doppler measurements of mesospheric momentum fluxes. *J. Atmos. Sci.*, **40**, 1321–1333.

Rüster, R., and I. M. Reid, 1990: VHF radar observations of the dynamics of the summer polar mesopause region. *J. Geophys. Res.*, **95**, 10 005–10 016.

Smith, S. A., D. C. Fritts, and T. E. VanZandt, 1987: Evidence for a saturated spectrum of atmospheric gravity waves. *J. Atmos. Sci.*, **44**, 1404–1410.

Thrane, E. V., O. Andreassen, T. A. Blix, B. Grandal, A. Brekke, C. R. Philbrick, F. J. Schmidlin, H.-U. Widdel, U. von Zahn, and F.-J. Lübken, 1985: Neutral air turbulence in the upper atmosphere. *J. Atmos. Terr. Phys.*, **47**, 243–265.

Tsuda, T., Y. Murayama, M. Yamamoto, S. Kato, and S. Fukao, 1990: Seasonal variation of momentum flux in the mesosphere observed with the MU radar. *Geophys. Res. Lett.*, **17**, 725–728.

Vincent, R. A., and I. M. Reid, 1983: HF Doppler measurements of mesospheric momentum fluxes. *J. Atmos. Sci.*, **40**, 1321–1333.

Wang, D.-Y., and D. C. Fritts, 1990: Mesospheric momentum fluxes observed by the MST radar at Poker Flat, Alaska. *J. Atmos. Sci.*, **47**, 1511–1521.

——, and ——, 1991: Evidence of gravity wave–tidal interaction observed near the summer mesopause at Poker Flat, Alaska. *J. Atmos. Sci.*, **48**, 572–583.